Hydrogen impurity in paratellurite α-TeO_2: Muon-spin rotation and *ab initio* studies

R. C. Vilão,* A. G. Marinopoulos, R. B. L. Vieira, A. Weidinger, H. V. Alberto, J. Piroto Duarte,† and J. M. Gil
CEMDRX, Department of Physics, University of Coimbra, P-3004-516 Coimbra, Portugal

J. S. Lord and S. F. J. Cox
ISIS Facility, Rutherford Appleton Laboratory, Chilton, Didcot, Oxon OX11 0QX, United Kingdom
(Received 25 February 2011; revised manuscript received 4 May 2011; published 1 July 2011)

We present a systematic study of isolated hydrogen in α-TeO_2 (paratellurite) by means of muon-spin spectroscopy measurements complemented by *ab initio* calculations based on density-functional theory (DFT). The observable metastable states accessible by means of the muon implantation allowed us to probe both the donor and the acceptor configurations of hydrogen, as well as to follow their dynamics. A shallow donor state with an ionization energy of 6 meV as well as a deep acceptor state are proposed, together with their atomic-level configurations and associated formation energies obtained from the DFT calculations. The latter show a tendency of interstitial hydrogen to bind strongly to bridging oxygen ions but also to coexist at sites deeper in the interior of the Te–O–Te rings with a more atomiclike character and a defect level in the gap. Atomlike interstitial muonium was observed; it has a hyperfine interaction of about 3.5 GHz. Charge and site changes with temperature are discussed.

DOI: 10.1103/PhysRevB.84.045201 PACS number(s): 71.55.Ht, 71.15.Nc, 61.72.−y, 76.75.+i

I. INTRODUCTION

The investigation of the role of hydrogen in semiconductors and oxides has assumed increasing and vital importance since the discovery that this ubiquitous impurity may play an active role as a source of *n*-type conductivity in ZnO: This prediction was made theoretically from calculations based on density-functional theory (DFT)[1] and first confirmed experimentally by muon-spin rotation (μSR) spectroscopy.[2] The identification of shallow-donor hydrogen levels was subsequently generalized to other related systems.[3–6] From the experimental point of view, the use of muonium ($\mu^+ e^-$, the hydrogenlike atom possessing a positive muon as the nucleus) as a light pseudoisotope of hydrogen has become standard in order to obtain information regarding the electronic states of hydrogen in materials.[7,8] The respective results compare well with those obtained with protons, for the very few cases allowing comparison.[3,9–11] These developments have recently prompted a thorough survey of the muonium states in most of the technologically relevant oxides.[12–14] Similarly, DFT calculations that aimed to identify the shallow or deep nature of hydrogen have also since been extended to many semiconductors and insulators.[15–20] Theoretical models have also been proposed attempting to predict the electrical activity of hydrogen, namely whether hydrogen can act as an electrically active impurity or an amphoteric impurity counteracting the prevailing conductivity;[13,15–18] these theoretical approaches usually rely upon a conversion level, the hydrogen $\epsilon(+/-)$ pinning level, claimed to be universal in an electrochemical scale for a wide selection of materials.[15,16,18]

α-TeO_2 (paratellurite) is a most interesting and relevant semiconducting oxide among nonlinear optical materials[21] and a promising active material for optical devices,[22–24] gas sensors,[25,26] and the search of neutrinoless β decay.[27] Its structure and vibrational and optical properties have also been recently the object of intensified research by *ab initio* DFT and molecular-orbital approaches.[21,28–30] High dielectric constants have also been reported,[30,31] which may include α-TeO_2 in the list of possible candidates for the replacement of SiO_2 as gate oxide material in highly miniaturized transistors.[32] The conductivity of α-TeO_2 has been the object of a limited number of studies mostly concentrated on the behavior at or above room temperature. Impurities seem to play a determinant role at room temperature, where *p*-type conductivity seems to be dominant,[33] although evidence for *n*-type conductivity has been found as well (Ref. 6 from Ref. 33). Hydrogen is present during the growth and is (nondeliberately) incorporated into the material and evidence of its interaction with other dopant ions and oxygen vacancies (V_O) has been suggested: Both the Cr^{3+}–V_O–2H center[34] and the V^{4+}–2H center[35] have been characterized. However, nothing is known about the configurations and dynamics of isolated hydrogen in α-TeO_2 and its effect on the electrical conductivity. This is a fundamental step to be undertaken before addressing the complexity related to the respective interaction with defects and impurities. The μSR spectroscopy is a privileged technique for this approach, since concentration of implanted positive muons basically corresponds to the extreme dilution limit. Therefore, the "isolated muon" at low temperature only interacts via charge carriers[36] and not directly with other defects or impurities unless these have very high concentrations corresponding to extreme positions of the sample Fermi level. Direct observation of the muon interaction with defects/impurities is usually observed only at temperatures much higher than liquid nitrogen temperature, upon muon diffusion.[37,38] For undoped samples, the usual concentration of electrons in the sample is sufficiently low to ensure that the local environment at the muon site is essentially intrinsic for cryogenic temperatures.

μSR, being a variant of ion-implantation techniques, can probe not only the stable muonium state corresponding to the absolute energy minimum at $T = 0$ K, but also other muonium states corresponding to higher-energy local minima, to be referred as metastable states. Transitions between states, in particular ionization, as a function of temperature were analyzed in this work with phenomenological Boltzmann

distributions.[13] This function describes the population of states in thermodynamical equilibrium and was used here to fit the s-shape-like change of the different fractions as a function of temperature. The main parameter extracted from these fits is the activation energy which has been then interpreted in physical terms.

In the following, we present the first systematic study of isolated hydrogen in α-TeO_2, through a synergistic investigation combining both experiment and *ab initio* DFT calculations. Experimentally, the modeling of isolated hydrogen was performed by means of the positive-muon analog and μSR spectroscopy. The *ab initio* DFT calculations consisted of the determination of the equilibrium configurations of hydrogen in all its charge states in the α-TeO_2 lattice and their corresponding formation energies as a function of the Fermi-level position in the band gap.

II. COMPUTATIONAL AND EXPERIMENTAL DETAILS

A. Crystal structure and theoretical framework

α-TeO_2 possesses tetragonal symmetry (space group No. 92, $P4_12_12$) with four formula units in the primitive unit cell. X-ray diffraction showed that α-TeO_2 has a distorted rutile structure whereby the rutile c-axis parameter is doubled.[39] The crystal is a network of corner-sharing TeO_4 units, where each tellurium has a fourfold asymmetric oxygen coordination with two oxygen atoms at shorter distances with respect to the rest.[28,29] The corresponding crystal structure is displayed in Sec. III D below, when discussing the hydrogen configurations.

The DFT calculations in the present study were based on the projector augmented wave (PAW) method as implemented in the VASP code.[40–43] The generalized-gradient approximation for exchange and correlation was employed and the Perdew-Burke-Ernzerhof (PBE) functional was used.[44] The crystalline wave functions were expanded in a plane-wave basis set limited by a kinetic energy cutoff of 500 eV. A Monkhorst-Pack[45] $9 \times 9 \times 9$ **k**-point mesh was used for the Brillouin-zone integrations for the bulk crystal. The calculated lattice constants, a and c, obtained from the structural optimization were equal to 4.96 Å and 7.64 Å, respectively. The internal parameters[28] were also determined: $x = 0.031$ for the tellurium and $(\alpha, \beta, \gamma) = (0.145, 0.256, 0.190)$ for the oxygen sublattice. These results are very similar to earlier DFT calculations[28,29] and in very good agreement with the existing x-ray diffraction data for the α-TeO_2 single crystal.[39]

In order to determine the equilibrium configurations of isolated, interstitial hydrogen in α-TeO_2, supercells with a total of 96 atoms were constructed by doubling the primitive-cell dimensions in all three directions. A coarser $3 \times 3 \times 3$ **k**-point mesh was used in these defect calculations. The formation energies, $E_{\text{form}}(H^q)$, for hydrogen in the charge state q were determined at $T = 0$ K as a function of the Fermi-level position, E_F, in the gap according to

$$E_{\text{form}}(H^q) = E_{\text{tot}}(H^q) - E_{\text{tot}}(\text{bulk}) - \mu_H + q(E_F + E_{\text{VBM}}). \quad (1)$$

In the above expression $E_{\text{tot}}(H^q)$ and $E_{\text{tot}}(\text{bulk})$ are the total energies of the supercell containing the hydrogen and the bulk-crystal supercell, respectively. μ_H is the hydrogen chemical potential taken as half the total energy of the hydrogen molecule and E_{VBM} is the valence-band maximum that provides the reference energy for the position of E_F. For the charged hydrogen states a homogeneous charge background was introduced to enforce overall charge neutrality.

For finite temperatures, the vibrational-entropy contributions should also be considered. Nonetheless, for reasonably low temperatures the use of internal energies in the calculation of formation energies is justified. In an earlier work,[46] the vibrational entropy contribution to the free energies was determined for a number of impurities in silicon oxide (quartz) and silicon: differences in formation entropies of $3k_B$ among various defect configurations were obtained. Taking an even larger magnitude of $4k_B$ for the present case, and considering the relevant temperature range in the experiments (up to 300 K) an upper bound of 0.2 eV for the change in free energies due to vibrational-entropy is obtained. This magnitude will not affect the conclusions drawn from the $T = 0$ K DFT calculations.

The minimum-energy path and associated energy barrier connecting two of the multiple configurations of the neutral state of hydrogen were determined by the nudged elastic-band (NEB) method.[47]

B. μSR experiments

Muon-spin rotation and relaxation experiments took place at the EMU instrument of the ISIS Facility, Rutherford Appleton Laboratory, United Kingdom, and at the DOLLY instrument of the Muon Spin Laboratory at the Paul Scherrer Institut, Switzerland.

In the experiments, a monocrystalline α-TeO_2 sample (obtained commercially from the MTI corporation) was used. Positive muons were implanted into the sample, the implanted muon spin polarization being parallel to the 100 axis. Conventional transverse-field and longitudinal-field measurements[48] were undertaken from liquid-helium temperature up to room temperature, and the respective experimental details are presented below. In order to reduce the spurious (background) events, both the flypast setup at ISIS[49] and the veto detector at PSI[50] were used. The sample was stored and handled in air. During the measurements, the sample was in low-pressure helium exchange gas. No significant change with ambient atmosphere is expected to occur for temperatures below 650 K.[33] Although no information is available about the concentration of dopants in the sample, we note that usual commercial samples of TeO_2 are expected to present aliovalent impurity concentrations of about 0.1 ppm,[51] which are too low in order to expect any direct interaction with the implanted muon.

In Fig. 1 we present typical transverse-field time spectra obtained for α-TeO_2 at PSI, at $T = 5$ K and at $T = 300$ K. An external transverse-field $B = 1.5$ mT was applied. A clear slightly damped oscillation at the Larmor frequency $\omega/2\pi = (\gamma_\mu/2\pi)B = 0.204$ MHz is observed, corresponding to muons in a diamagnetic environment. In addition, a strong relaxation is present in the first few hundred nanoseconds, which we assign to muons in a paramagnetic environment, as discussed below. We have fitted the time spectra with the sum of two components,

$$A(t) = A_{\text{slow}} e^{-\lambda_{\text{slow}} t} \cos(\omega t + \phi_{\text{slow}}) + A_{\text{fast}} e^{-\lambda_{\text{fast}} t}, \quad (2)$$

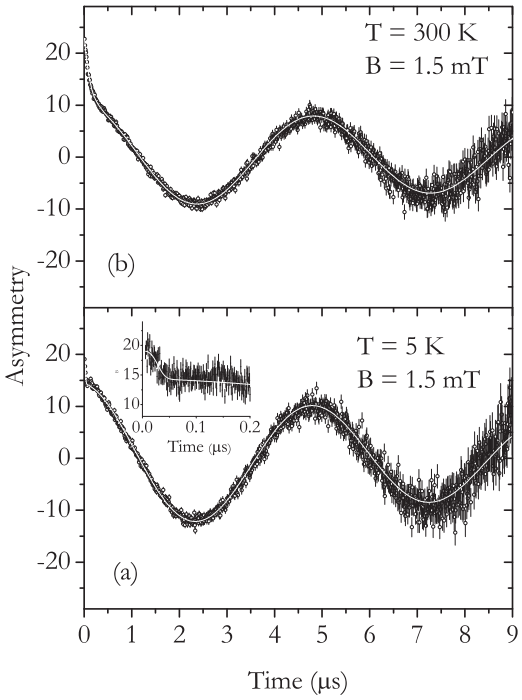

FIG. 1. Muon spin asymmetry as a function of time, in transverse geometry ($B = 1.5$ mT), at $T = 5$ K (below), and at $T = 300$ K (observed at PSI). A clear nearly undamped oscillation at the Larmor frequency is observed, which amounts to ~60% of the initial muon spin polarization at $T = 5$ K and to ~40% of the initial muon spin polarization at $T = 300$ K. A strongly relaxed signal is observed in the first few hundred nanoseconds. Lines are fits as discussed in the text.

an oscillating and a nonoscillating part, both with an exponentional damping, where the subscripts "slow" and "fast" stand for the slowly relaxing and the fast relaxing component, respectively. Some spectra were also analyzed with different damping functions for the fast relaxing component as described in the text. Note that the fast decay is so fast that Eq. (2) is indistinguishable from

$$A(t) = [A_{\text{slow}} e^{-\lambda_{\text{slow}} t} + A_{\text{fast}} e^{-\lambda_{\text{fast}} t}] \cos(\omega t + \phi_{\text{slow}}). \quad (3)$$

The presence of these two relaxing components presents an experimental problem: On one hand, a clear definition of the slowly relaxing diamagnetic component benefits from the large time window available only at ISIS; on the other hand, the pulsed nature of ISIS beam limits the observation of the highly relaxing component, which is best followed at PSI, with its quasicontinuous beam. A coherent overall picture can therefore be obtained only from a conjugation of the data obtained at both facilities.

Below 125 K, the two signals appear to represent distinct diamagnetic and paramagnetic fractions. Thus, in Fig. 1(a) we attribute the fast decay ($\lambda_{\text{fast}} > 30\ \mu\text{s}^{-1}$) to an overdamped precession signal of triplet-state muonium, promptly formed but very short lived. In this regime, other forms of the fast relaxation function fit equally well, for example, Gaussian or even compressed exponentials such as $\exp[-(\lambda_{\text{fast}} t)^3]$, which we found to provide the best description for the data in this temperature range.

Above 125 K, a single Larmor precession signal with biexponential relaxation [cf. Eq. (3)] appears more appropriate to our physical interpretation of this regime. In Fig. 1(b), the initial fast decay is certainly exponential, but with a rate not exceeding 8 μs^{-1}. It could represent muonium, whose formation is delayed on this time scale, or muonium that is subject to charge exchange on a much faster time scale.

Measurements in longitudinal geometry[48] were also undertaken at ISIS at $T = 6$ K in order to characterize the hyperfine interaction of the paramagnetic species involved. In order to avoid complications arising from extreme variations of the maximum instrumental asymmetry in the flypast setup, the sample was mounted in a large silver plate. The diamagnetic component arising from silver was obtained from a calibration with a hematite replica of the TeO_2 sample mounted on the same silver plate. A calibration of the (slight) variation of the maximum instrumental asymmetry with applied longitudinal field was obtained with the silver plate. The time spectra were fitted to a single exponential decay.

III. RESULTS AND DISCUSSION

Figure 2 displays the fractions as a function of temperature between 5 K and 300 K. These have been obtained by comparison of the fitted asymmetries A_{slow} and A_{fast} to the maximum instrumental asymmetry, as obtained from a calibration with silver. The dominant part is the slowly relaxing fraction (Mu^+ or Mu^-) which is present at all temperatures. The fast relaxing fraction (associated to Mu^0) amounts to about 20% at low temperatures, then decreases at intermediate temperatures and increases again toward 300 K. A similar polarization fraction of about 20% is missing at low temperatures but is recovered continuously with increasing temperatures. A remarkable feature of the data is the peak in the slowly relaxing fraction around 125 K and the corresponding dip in the fast relaxing fraction, indicating an interconversion process of the two fractions.

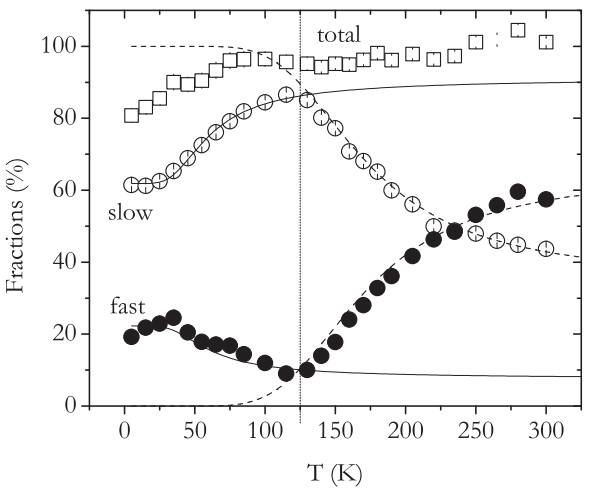

FIG. 2. Temperature dependence of the slow component (open circles), the fast component (solid circles) and total fraction (open squares), as observed at PSI, for an applied transverse field $B = 1.5$ mT. A clear (inter)conversion process occurs between these two components. Lines are fits as discussed in the text.

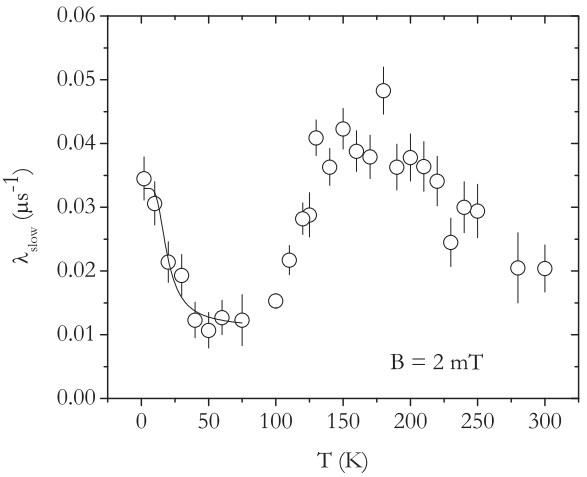

FIG. 3. Temperature dependence of the slow Lorentzian relaxation λ_{slow}, observed at ISIS in transverse-field experiments ($B = 2$ mT). The solid line below 75 K is a fit to an activated process which we assign to the ionization of a shallow donor. We associate the peak around $T = 175$ K to charge fluctuations arising from the (inter)conversion process.

Figure 3 displays the relaxation rate λ_{slow} of the slowly relaxing fraction as a function of temperature. The overall values are very low and could be measured only at ISIS with the long time window. A transverse field $B = 2$ mT was used. Two features are seen. At low temperatures a slightly enhanced relaxation is observed which decreases quickly with increasing temperatures. This part is attributed to a very weak hyperfine interaction which disappears after ionization of a shallow muonium state (see Sec. III A below). The second feature at around 175 K may be associated with charge fluctuations (see Sec. III C 2 below).

Figure 4 shows the relaxation rate λ_{fast} of the fast relaxing fraction as a function of temperature. Such a high relaxation can be caused only by a hyperfine interaction and thus indicates the presence of muonium, either directly formed as the muon

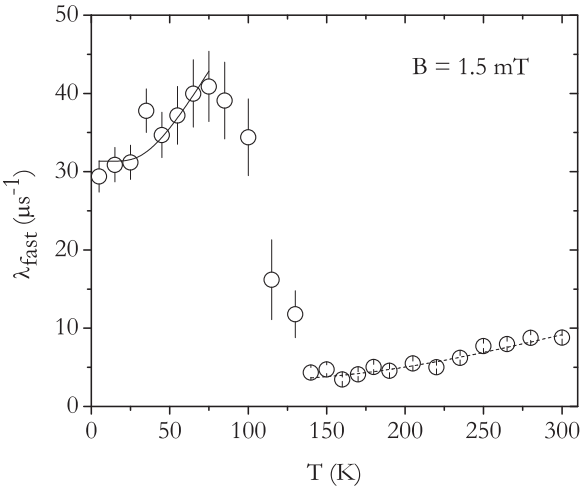

FIG. 4. Temperature dependence of the paramagnetic relaxation λ_{fast} observed at PSI in transverse-field experiments ($B = 1.5$ mT). The lines are simulations to the 13-meV (solid line) and 63-meV (dashed line) conversion processes discussed in the text.

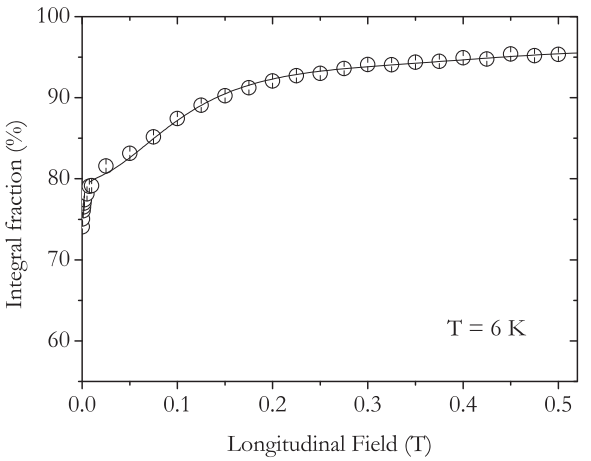

FIG. 5. Dependence of the integral fraction with an applied longitudinal field, at $T = 6$ K, observed at ISIS. The line is a fit with a fully isotropic state as described in the text.

stops in the sample or created later via charge-state changes. The signal is defined by a few data points at the beginning of the time spectra only and therefore the extracted parameters depend on the actual relaxation function used, giving rise to systematic uncertainties not included in the error bars shown in the figure.

Figure 5 shows the recovery of the integral muon spin polarization as a function of the applied longitudinal magnetic field at 6 K. The main recovery occurs in the field range between about 50 and 500 mT, indicating the decoupling of a muonium hyperfine interaction close to the vacuum value. The fitting curve in Fig. 5 has been obtained using the QUANTUM program[52] by assuming the presence of an isotropic hyperfine interaction $A_{iso} = 3.5(1)$ GHz.

A. Shallow-donor state and the donor level

We assign the decrease of λ_{slow} in Fig. 3 with increasing temperature to the ionization of shallow muonium. In this state the present DFT calculations show that hydrogen (and therefore muonium) binds strongly to an oxygen ion of the lattice, forming a covalent bond (cf. Sec. III D); this configuration is referred to as bond configuration in the following. In favor of this assignment, we may argue that the strongest competing description, in terms of the decrease of relaxation felt by a diffusing particle in the presence of the magnetic field created by the nuclear magnetic moments[53] (motional narrowing), can be discarded. First, the abundance of magnetic moments in TeO_2 is very low (the only significant natural isotope is ^{125}Te, with 7% abundance), and we may expect the corresponding Gaussian relaxation not to exceed $0.01\mu s^{-1}$, from calculations of the second moment of the magnetic field arising from the nuclear moments[53] at the hydrogen sites determined from the *ab initio* calculations presented below in this work. The origin of the observed relaxation is therefore electronic.

The formation of shallow muonium, that is, of a bound hydrogenic state of an electron to the positive muon with an extremely small hyperfine interaction A (around few hundred kHz) in principle gives rise to two additional frequency lines

placed symmetrically around the diamagnetic line $\omega_\mu/2\pi$, at $\omega_\mu/2\pi \pm A/2$. However, if spin-flip dynamics exists or the instrumental resolution is not enough to resolve these lines, the effect will be that of a single broadened line at $\omega = \omega_\mu$.[13] In the static case, the value of the broadening is of the order of magnitude of the hyperfine interaction, which points to a hyperfine interaction with an order of magnitude about 10 kHz, which compares with similar values for other oxides.[13] The decrease of this broadening with increasing temperature thus corresponds to the ionization of the bound shallow muonium state in the donorlike process:

$$\mathrm{Mu}_\mathrm{D}^0 \rightarrow \mathrm{Mu}_\mathrm{D}^+ + e_\mathrm{CB}^-. \tag{4}$$

In order to fit the decrease in λ_{slow}, we took the weighted average of the relaxation λ_+ of the muons in the pure diamagnetic state, and of the relaxation λ_0 of the muons in the shallow paramagnetic state,

$$\lambda_d = f_0\lambda_0 + f_+\lambda_+, \tag{5}$$

where the formation probability f_0 of the shallow paramagnetic state is assumed to have the phenomenological Boltzmann dependence,[13]

$$f_0(T) = \frac{1}{1 + N\exp(-E_a/k_\mathrm{B}T)}, \tag{6}$$

where E_a is the activation energy of the process, k_B is the Boltzmann constant, and the empirical parameter N relates to the density of states. The normalized formation probability of the corresponding diamagnetic state obeys $f_+ = 1 - f_0$. We note that these formation probabilities are normalized to the total diamagnetic fraction f_d observed at low temperatures. We also note that for $\lambda_+ = 0$, one obtains (for a fixed λ_0) the proportionality between the relaxation rate λ_d and the paramagnetic fraction f_0, as used in Ref. 13. In the fit shown in Fig. 3, the relaxation of the diamagnetic state was fixed to $\lambda_+ = 0.01\ \mu s^{-1}$, and an activation energy $E_a = 6(2)$ meV [with $N = 3(2) \times 10$, $\lambda_0 = 0.033(2)$ MHz] was obtained.

From this value, and using $\epsilon = 24(1)\epsilon_0$ (Refs. 30 and 31) for the static dielectric constant in α-TeO_2, we may estimate[13,14] the electron effective mass to be $m^* = 0.3(1)m_0$ and the hyperfine interaction to be around 0.05 MHz (corresponding to a Bohr radius of about 50 Å).

B. Atomlike (deep) muonium

In longitudinal-field experiments performed at $T = 6$ K, a clear repolarization curve is seen (Fig. 5), corresponding to a hyperfine interaction of about 3.5 GHz. The interaction is isotropic or almost isotropic and its value amounts to about 78% of the vacuum value. This is the signature of an atomlike state with little interaction with the surroundings. It is usually assumed that this so-called deep or normal muonium resides at an open interstitial site in the lattice.[54] Indeed, the DFT calculations determined a higher-energy metastable configuration of neutral hydrogen with the latter residing deeper in the interior of the ring structure of the lattice (cf. Sec. III D below).

From such a state, in low transverse field, the singlet-triplet transition frequency of about 3.5 GHz is far too high to be resolved, so that half the polarization is lost. The other half would normally be seen as an intratriplet precession signal, with frequency 21 MHz at 1.5 mT. In the present case it appears to be damped in less than one cycle, mainly reflecting the short lifetime of the quasiatomic state. The equality of the missing and fast-decaying fractions support this interpretation, accounting in total for 40% of the incoming muons.

C. Conversion dynamics

As discussed above, at the lowest temperatures, about 60% of the muons form the donor configuration and about 40% form the atomlike muonium. However, this ratio is not constant but changes with temperature as evidenced by the increase and decrease of the slowly relaxing component, with a maximum at about 125 K. We assign the increase to a conversion of paramagnetic deep muonium to diamagnetic muonium (which can correspond to Mu^+ or Mu^-, not specifying the charge state at this stage). The decrease is then assigned to a reverse reaction: $\mathrm{Mu}^{+,-}$ converts to Mu^0. In the reverse reaction, charge fluctuations seem to play a non-negligible role. In the following we concentrate the discussion on the fractions represented in Fig. 2, from which an activation energy for the ongoing processes can be extracted. We refrain from the corresponding analysis of the relaxations shown in Figs. 3 and 4, which would require a rather detailed model for the ongoing processes, which we can only hint at. The clarification of such processes requires an extensive research program built upon the results of the current work, in order to clarify the specific processes involved and build an adequate model such as the one currently existing for intrinsic silicon.[10] A comprehensive model should also include indirect interaction with defects and impurities such as those known in other related systems.[36,55] However, the temperature dependence of the fractions contains already the basic feature relative to the conversion of the muonium states present.

1. *Conversion of Mu^0 to $Mu^{+,-}$ ($T < 125$ K)*

Experimentally we cannot distinguish between Mu^+ and Mu^- and therefore no definite assignment can be made to the final state being formed. Again, we assume a phenomenological Boltzmann partition between the two configurations

$$f_{\mathrm{fast}}(T) = \frac{1}{2}\frac{f_p}{1 + N_1\exp(-E_1/k_\mathrm{B}T)}, \tag{7}$$

$$f_{\mathrm{slow}}(T) = \frac{f_p N_1\exp(-E_1/kT)}{1 + N_1\exp(-E_1/k_\mathrm{B}T)} + f_d, \tag{8}$$

where f_d and f_p are the total formation probabilities of the diamagnetic and atomlike paramagnetic configurations, respectively, and $f_d + f_p = 1$ or $f_p = 1 - f_d$. E_1 is the activation energy of the process, k_B is the Boltzmann constant, and the empirical parameter N_1 relates to the density of states. The index 1 is used here to distinguish the parameters used in Eqs. (7) and (8) from those used for the processes described in the next paragraph, where we use index 2. The factor 1/2 in the Eq. (7) accounts for the fact that only half of the Mu^0 frequencies are visible for deep muonium, the other half of the transitions being not detected due to their high frequencies. The simultaneous fit of Eqs. (7) and (8) to the data below $T = 125$ K

is represented in Fig. 2 (full lines), yielding $f_d = 61.6(5)\%$, $N_1 = 6(1)$, and an activation energy $E_1 = 13(1)$ meV.

A possible process for the transition of Mu^0 to Mu^+ is the site change of interstitial muonium to the bond donor configuration, accompanied by a loss of the electron. The activation energy ($E = 13$ meV) extracted from the increase of the slowly relaxing fraction would then represent the barrier height for the conversion. This process would then correspond to a deep to shallow conversion of the neutral state, with simultaneous ionization above 50 K.

This process seems a very plausible explanation and is consistent as well with our DFT-NEB calculations for hydrogen, where a very low barrier is obtained. However, a problem arises for the temperatures above 125 K, where apparently the reverse reaction occurs. The bond donor configuration is a very stable situation and a re-formation of the higher-energy interstitial state seems unlikely: It would require the breaking of a strong covalent bond with oxygen. The present DFT-NEB calculations for the barrier of the path leading to such a re-formation provide a magnitude of 1.4 eV, suggesting this to be a very difficult process.

Therefore, we consider also the possibility of Mu^- formation. This process was proposed in Refs. 56 and 57 for the ZnSe case and the current DFT calculations depict it as very probable here as well, since the existence of a stable negatively charged hydrogen state in the deep interstitial geometry is predicted (see Sec. III D below). In this interpretation one assumes that radiolytically produced conduction electrons are temporarily stored at the native donors in these heavily compensated materials and liberated at the temperature where ionization occurs. These electrons can then be captured at interstitial muonium to form Mu^-. In this case the 13-meV activation energy extracted from the fit in Fig. 2 below 125 K represents the ionization energy of the native donors.

2. *Conversion of $Mu^{+,-}$ to Mu^0 ($T > 125$ K)*

Above 125 K, the slowly relaxing diamagnetic muonium fraction decreases (Fig. 2), meaning that this configuration becomes unstable. The high relaxation value of the fast relaxing component (Fig. 4) requires that a deep muonium state is formed, at least temporarily. We interpret the decay of the slowly relaxing component in Fig. 2 as due to the reverse process and extract an activation energy by fitting the fractions with Boltzmann distributions analogous to the model described in Eqs. (7) and (8) [where the factor 2 in Eq. (7) is now removed to take into account that the entire muon polarization is now observed]. The resulting simultaneous fit to the two fractions for $T > 125$ K is represented in Fig. 2 (dashed lines) and yields $f_d = 33(3)\%$, $N_2 = 66(30)$, and an activation energy of 63(5) meV.

In case of the reactivation of muonium from the bond site to the interstitial site, this value would represent the energy difference of the neutral muonium in the two configurations, respectively. 63 meV seems too low for this level difference, compared to 1.3 eV predicted by DFT (see Sec. III D below).

For the Mu^- configuration, an instability is more plausible since the second electron in Mu^- may easily be lost either to the valence band filling holes if present[58] or to the conduction band.[56] Again, 63 meV seems too low for the latter case, since the theoretical DFT predictions place the thermodynamic $\epsilon(0/-)$ level about midgap, and the $\epsilon(0/-)$ level associated to the interstitial hydrogen configuration even lower (see Fig. 6). In the former case (hole capture), the activation energy corresponds to the activation energy of the native acceptors and 63 meV appears as a most sensible value.

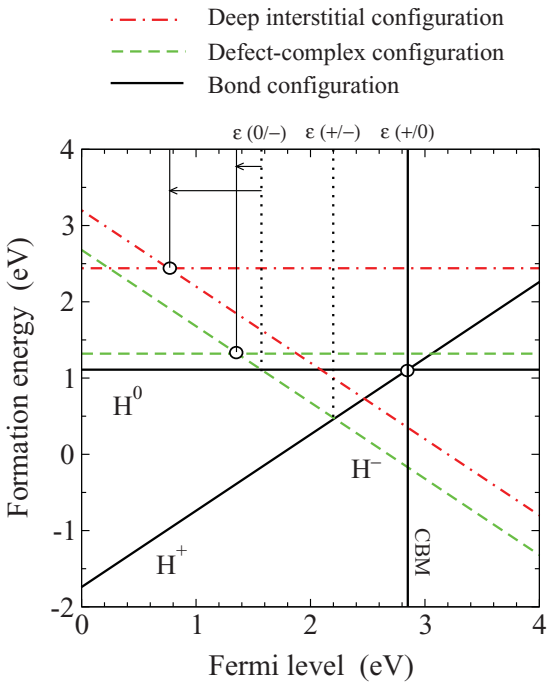

FIG. 6. (Color online) Formation energies of the different charge states of hydrogen versus Fermi-level position in the band gap. The energies for all multiple minimum-energy configurations discussed in the text are included as well, with corresponding labels shown above the plot. The thermodynamic defect transition levels, $\epsilon(q,q')$, are denoted by the vertical dotted lines. The positions of the acceptor levels $\epsilon(0/-)$ among the H^0 and H^- states stable at different geometric configurations are also explicitly shown by the arrows. The solid vertical line, marked as CBM, denotes the theoretical DFT conduction-band minimum. The reference energy for the Fermi level is set at the valence band maximum.

D. DFT study: Hydrogen configurations and formation energies

Hydrogen in all its charge states (H^0, H^+, and H^-) was initially placed in various positions in the 96-atom bulk-crystal supercells. The equilibrium configurations were then determined by minimization of the total internal energy. For every charge state the resulting minimum-energy configurations were identified, exploring also the possibility of coexistence of multiple energy minima. The corresponding formation energies are shown in Fig. 6 as a function of the Fermi-level position in the band gap, for all different minimum-energy configurations that hydrogen can exist for each of its charge states. The thermodynamic transition levels $\epsilon(q/q')$, defined by the value of the Fermi level where the charge states q and q' have equal energies, are also indicated by the dotted vertical lines. To determine these levels we considered only the lowest-energy configurations for each charge state. It can be seen that the donor level $\epsilon(+/0)$ lies higher in the

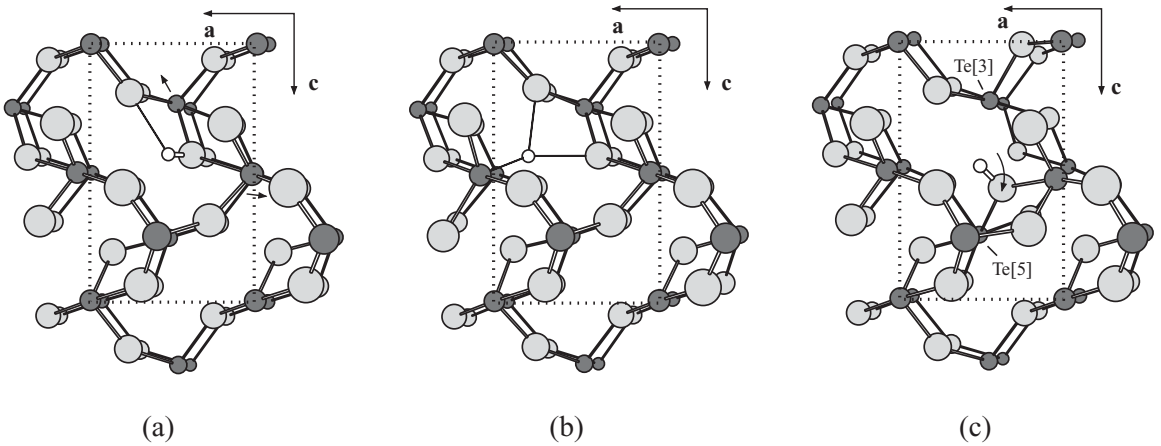

FIG. 7. Minimum-energy configurations of isolated hydrogen (small white circle) in α-TeO_2, shown in a projection parallel to the **b**-lattice vector. Oxygen and tellurium ions are depicted as the larger and lighter (smaller and darker) circles, respectively. Dotted lines denote the bulk-crystal repeating unit. (a) Bond configuration; (b) High-energy deep interstitial configuration; (c) Defect-complex-acceptor-like configuration.

gap compared to the acceptor level $\epsilon(0/-)$. This inequality suggests that the present DFT calculations predict hydrogen to be a negative-U defect in α-TeO_2, where the neutral H^0 state is never thermodynamically stable at any value of the Fermi level.[13] It should also be pointed out that the finding that the equilibrium pinning level $\epsilon(+/-)$ is within the gap means that hydrogen is not a source of doping in α-TeO_2.[18] Nonetheless, both H^0 and H^- can exist in more than one configuration in the lattice (see Fig. 6) and the existence of these higher-energy metastable configurations is still relevant, especially when comparing with μSR measurements, since the latter access nonequilibrium processes occurring at a very short time scale. For this reason, the formation energies associated with all existing multiple configurations are also shown in Fig. 6 and are discussed below. A consequence of this is that new displaced transition levels become possible that connect the higher-energy charge states of hydrogen for each different geometrical configuration. These are indicated by arrows in Fig. 6, where it can be seen that the acceptor level $\epsilon(0/-)$ is progressively displaced closer to the valence-band edge.

Interstitial hydrogen for all charge states displayed a strong tendency to bind to the bridging oxygen atoms (rendering them threefold coordinated) with a formation of a strong covalent O–H bond with a length of 0.98 Å. The corresponding equilibrium configuration for hydrogen in the positive charge state, H^+, is shown in Fig. 7(a). The depicted projection is parallel to the lattice vector b, where the network of six-membered Te–O–Te rings is clearly visible. The O–H bond is oriented perpendicular to the c axis and is shown by the thicker segment in the figure. Inspection of the local environment of H^+ revealed that H^+ forms an additional longer bond (2.13 Å) with another oxygen ion. The latter shares a common tellurium neighbor with the primary oxygen that H^+ binds to [Fig. 7(a)]. The incorporation of H^+ also does not entail breaking of a host Te–O bond, similarly to other rutile-structured oxides such as SnO_2 and TiO_2.[15,19,20,59] The close proximity of H^+ to its binding oxygen only repels the two tellurium nearest neighbors of the latter by approximately 0.25 Å each (the corresponding displacements are depicted by the arrows in Fig. 7). The H^+ configuration does not introduce any defect levels in the band gap.

For the case of a neutral supercell, hydrogen was also found to adopt this bond configuration. Again, no deep state in the gap appears: The additional electron occupies an energy level that is resonant with the conduction band, rendering hydrogen effectively ionized with its electron in a delocalized state. The impurity center is therefore an ionized hydrogen with the electron bound to the center in a hydrogenic effective-mass state. The calculated donor level $\epsilon(+/0)$ is nearly degenerate with the conduction-band minimum, CBM (Fig. 6). These findings thus suggest that the bond configuration very likely corresponds to the shallow muonium state observed in μSR with an estimated Bohr radius of about 50 Å (see Sec. III A).

By exploring further the configurational space of hydrogen in the lattice in the neutral supercell (still referred to as H^0, for conventional purposes) we found that H^0 possesses another stable configuration of higher energy (by 1.3 eV) where the hydrogen atom resides at an interstitial site deeper in the interior of the ring [see Fig. 7(b)]. More specifically, hydrogen is located close to its nearest tellurium ion at a distance of 1.75 Å, with the next-nearest neighbors being two oxygen ions across the ring at distances in the 1.90-to-2.20-Å range. Calculations (with the NEB method) of the minimum-energy path connecting the two multiple configurations of H^0, namely, the lower-energy bond site and the deep interstitial site, revealed that a very low energy barrier (of the order of 0.1 eV, practically within the numerical accuracy of the calculations) is needed for H^0 to escape from the higher-energy site toward its global minimum-energy bond site. The interstitial configuration is a deep state with the electron occupying a deep defect level located 1.2 eV above the VBM. The electron charge density of this level is plotted in Fig. 8(a). It can be seen that the state is relatively localized at the hydrogen itself in an approximately spherically symmetric charge distribution, but carries also considerable weight at ions of its immediate vicinity, most notably its tellurium nearest neighbor. Therefore, it has an atomlike character but with strong influences from the local environment as

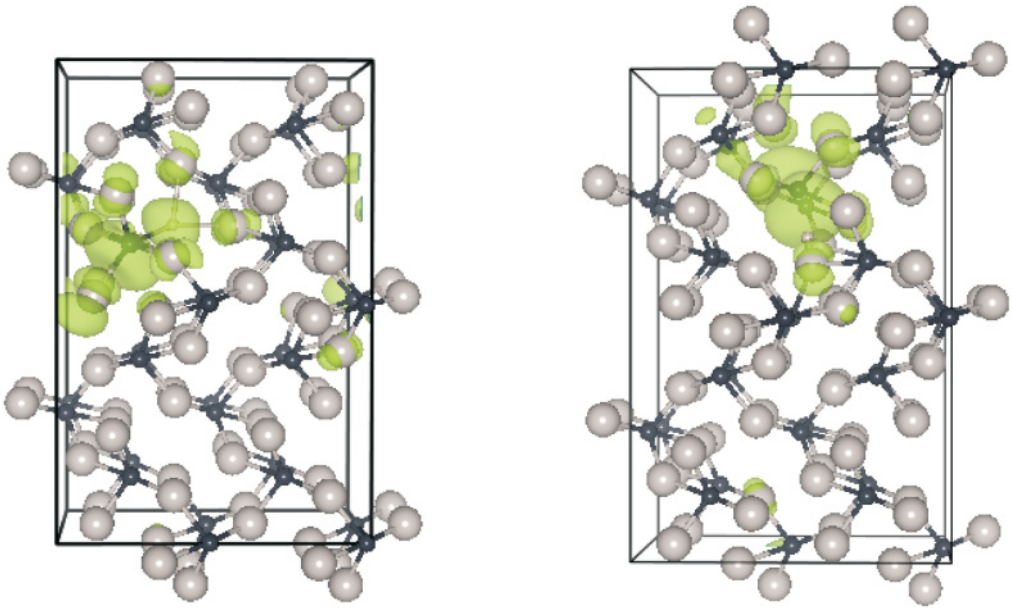

(a) (b)

FIG. 8. (Color online) Isosurfaces (in color) of the electron charge densities for the defect level in the gap in the higher-energy deep interstitial H^0 configuration (a) and in the intermediate-energy defect-complex H^0 configuration (b). The full supercell is shown for both cases, in a projection parallel to the **b**-lattice vector.

well. We suggest that the deep isotropic muonium found in the experimental results and discussed in the Sec. III B corresponds to this configuration. The calculations also show that this configuration is stable upon the subsequent electron capture by this center, converting it into a stable H^- state. Concerning the negatively charged H^- case, however, two different configurations are possible, as we now discuss.

Indeed, for the negatively charged hydrogen, H^-, the previously described interstitial configuration was also found to be stable. In contrast to H^0 and H^+, however, the bond configuration discussed above has a higher energy (almost by 1 eV) and it was found to be unstable under small perturbations, especially with respect to displacements of the oxygen ion (participating in the OH^- bond) along the *c* axis [see Fig. 7(c)]. This instability leads to a new stable H^- configuration of lower energy with respect to the interstitial state (Fig. 6). This H^- state, depicted in Fig. 7(c), is a rather extended defect complex. It comprises an OH^- bond, which this time is no longer perpendicular to the *c* axis, and a pair of under- and overcoordinated tellurium ions in its immediate vicinity, Te[3] and Te[5]. The oxygen ion participating in the OH^- bond has displaced considerably from its initial position in the lattice, leaving behind a threefold coordinated tellurium (Te[3]) and creating an overcoordinated one (Te[5]). This negatively charged state possesses a defect level deep in the band gap, occupied by two electrons.

We further tested the stability of this defect complex by subtracting one and two electrons from it. Whereas the positively charged state was unstable, the defect-complex configuration persists (with some changes in the local structure) as a neutral state. This state, therefore, is the third stable H^0 configuration in α-TeO_2 with a singly occupied deep level in the gap and an energy slightly higher than the energy of the H^0 bond state discussed earlier (see Fig. 6). The charge-density distribution for this level, shown in Fig. 8(b), is localized near the O–H^- bond and displays a strong asymmetry with a large weight on the undercoordinated tellurium ion, Te[3].

IV. CONCLUSIONS

The present study is a comparative work of the incorporation and dynamics of isolated interstitial hydrogen in α-TeO_2 by means of muon experiments and DFT calculations.

In the theoretical DFT part, in addition to the lowest-energy configurations of hydrogen for each of its charge states, higher-energy metastable states were also determined since they can be relevant and accessible to the implanted muons. Six minimum-energy hydrogen states are predicted together with their level crossings. These six states are grouped in three geometrical configurations: a donor configuration with the hydrogen forming a short covalent bond to an oxygen ion of the lattice, encountered also in many other oxides, and two other configurations with deep defect levels in the gap: a defect-complex acceptorlike configuration with the hydrogen again strongly bound to an oxygen and a third interstitial one with the hydrogen occupying a position deeper in the ring structure of the α-TeO_2 lattice.

Experimentally, both the donor and the higher-energy interstitial configurations have been observed. We have no experimental indication of the formation of the acceptorlike configuration where the muonium is strongly bound to the lattice. We suppose that the formation of this configuration is hindered by the requirement of the strong geometrical rearrangements to form it.

In the donor configuration, muonium is mainly ionized (Mu^+) but a faint indication of a hyperfine interaction remains, indicating that a weakly bound electron is present. From the disappearance of this interaction with temperature, the $\epsilon(+/0)$ conversion level can be located near the conduction band edge within a range of about ~6 meV. This result is consistent with the theoretical DFT prediction.

The formation of the deep interstitial configuration is evidenced by the observation of atomiclike deep muonium with a hyperfine interaction of about 3.5 GHz, corresponding to about 78% of the vacuum value. None of the two other neutral muonium configurations would show this characteristic. The experimentally observed gradual increase of the diamagnetic fraction with temperature up to 125 K is attributed to electron capture by the interstitial muonium forming Mu^-, the decrease of this fraction above 125 K to the loss of the second electron forming Mu^0 again. However, this interpretation is not unique and alternative models are also discussed. The combined experimental and DFT study provides a quite complete picture of the basic behavior of isolated interstitial hydrogen in α-TeO_2.

ACKNOWLEDGMENTS

The technical help of the μSR facility scientists at ISIS and PSI is gratefully acknowledged. The computing resources of the Department of Physics of the University of Coimbra were used, including the Milipeia cluster at the Laboratory for Advanced Computing. This work was supported by the program COMPETE: FCOMP-01-0124-FEDER-010450 and by the Portuguese Fundação para a Ciência e a Tecnologia (FCT) under the Ciência 2007 program and through Project No. PTDC/FIS/102722/2008.

*ruivilao@fis.uc.pt

†Also at E.S.Te.S.C., Polytechnic Institute of Coimbra, P-3040-854 Coimbra, Portugal.

[1] C. G. Van de Walle, Phys. Rev. Lett. **85**, 1012 (2000).

[2] S. F. J. Cox, E. A. Davis, S. P. Cottrell, P. J. C. King, J. S. Lord, J. M. Gil, H. V. Alberto, R. C. Vilão, J. Piroto Duarte, N. Ayres de Campos, A. Weidinger, R. L. Lichti, and S. J. C. Irvine, Phys. Rev. Lett. **86**, 2601 (2001).

[3] J. M. Gil, H. V. Alberto, R. C. Vilão, J. Piroto Duarte, N. Ayres de Campos, A. Weidinger, J. Krauser, E. A. Davis, S. P. Cottrell, and S. F. J. Cox, Phys. Rev. B **64**, 075205 (2001).

[4] E. A. Davis, S. F. J. Cox, R. L. Lichti, and C. G. Van de Walle, Appl. Phys. Lett. **82**, 592 (2003).

[5] R. C. Vilão, H. V. Alberto, J. M. Gil, J. P. Piroto Duarte, N. Ayres de Campos, A. Weidinger, and M. V. Yakushev, Physica B **340**, 965 (2003).

[6] H. V. Alberto, A. Weidinger, R. C. Vilão, J. P. Duarte, J. M. Gil, J. S. Lord, and S. F. J. Cox, Phys. Rev. B **81**, 245205 (2010).

[7] R. L. Lichti, K. H. Chow, J. M. Gil, D. L. Stripe, R. C. Vilão, and S. F. J. Cox, Physica B **376**, 587 (2006).

[8] R. L. Lichti, K. H. Chow, and S. F. J. Cox, Phys. Rev. Lett. **101**, 136403 (2008).

[9] Vl. Kolkovsky, V. Kolkovsky, K. B. Nielsen, L. Dobaczewski, G. Karczewski, and A. N. Larsen, Phys. Rev. B **80**, 165205 (2009).

[10] B. Hitti, S. R. Kreitzman, T. L. Estle, E. S. Bates, M. R. Dawdy, T. L. Head, and R. L. Lichti, Phys. Rev. B **59**, 4918 (1999).

[11] C. Herring, N. M. Johnson, and C. G. Van de Walle, Phys. Rev. B **64**, 125209 (2001).

[12] S. F. J. Cox, J. S. Lord, S. P. Cottrell, J. M. Gil, H. V. Alberto, A. Keren, D. Prabhakaran, R. Scheuermann, and A. Stoykov, J. Phys. Condens. Matter **18**, 1061 (2006).

[13] S. F. J. Cox, J. L. Gavartin, J. S. Lord, S. P. Cottrell, J. M. Gil, H. V. Alberto, J. Piroto Duarte, R. C. Vilão, N. Ayres de Campos, D. J. Keeble, E. A. Davis, M. Charlton, and D. P. van der Werf, J. Phys. Condens. Matter **18**, 1079 (2006).

[14] P. D. C. King, R. L. Lichti, Y. G. Celebi, J. M. Gil, R. C. Vilão, H. V. Alberto, J. Piroto Duarte, D. J. Payne, R. G. Egdell, I. McKenzie, C. F. McConville, S. F. J. Cox, and T. D. Veal, Phys. Rev. B **80**, 081201 (2009).

[15] Ç. Kiliç and A. Zunger, Appl. Phys. Lett. **81**, 73 (2002).

[16] C. G. Van de Walle and J. Neugebauer, Nature (London) **423**, 626 (2003).

[17] J. Robertson and P. W. Peacock, Thin Solid Films **445**, 155 (2003).

[18] C. G. Van de Walle, Physica B **376-377**, 1 (2006).

[19] K. Xiong, J. Robertson, and S. J. Clark, J. Appl. Phys. **102**, 083710 (2007).

[20] A. K. Singh, A. Janotti, M. Scheffler, and C. G. Van de Walle, Phys. Rev. Lett. **101**, 055502 (2008).

[21] S. Suehara, P. Thomas, A. P. Mirgorodsky, T. Merle-Méjean, J. C. Champarnaud-Mesjard, T. Aizawa, S. Hishita, S. Todoroki, T. Konishi, and S. Inoue, Phys. Rev. B **70**, 205121 (2004).

[22] E. Yu. Vorontsova, R. M. Grechishkin, I. A. Kaplunov, A. I. Kolesnikov, V. Ya. Molchanov, I. V. Talyzin, and S. A. Tret'yakov, Opt. Spectrosc. **104**, 886 (2008).

[23] V. A. Bagan, B. L. Davydov, and I. E. Samartsev, Quantum Electron. **39**, 73 (2009).

[24] S. Beke, T. Kobayashi, K. Sugioka, K. Midorikawa, and J. Bonse, Int. J. Mass Spectrom. **299**, 5 (2011).

[25] Z. Liu, T. Yamazaki, Y. Shen, T. Kikuta, N. Nakatani, and T. Kawabata, Appl. Phys. Lett. **90**, 173119 (2007).

[26] T. Siciliano, A. Tepore, G. Micocci, A. Genga, M. Siciliano, and E. Filippo, Sens. Actuators B **138**, 207 (2009).

[27] C. Arnaboldi, C. Brofferio, A. Bryant, C. Bucci, L. Canonica, S. Capelli, M. Carrettoni, M. Clemenza, I. Dafinei, S. Di Domizio, F. Ferroni, E. Fiorini, Z. Ge, A. Giachero, L. Gironi, A. Giuliani, P. Gorla, E. Guardincerri, R. Kadel, K. Kazkaz, L. Kogler, Y. Kolomensky, J. Larsen, M. Laubenstein, Y. Lim, C. Maiano, M. Martinez, R. Maruyama, S. Nisi, C. Nones, Eric B. Norman, A. Nucciotti, F. Orio, L. Pattavina, M. Pavan, G. Pessina, S. Pirro, E. Previtali, C. Rusconi, Nicholas D. Scielzo, M. Sisti, Alan R. Smith, W. Tianm, M. Vignati, H. Wang, and Y. Zhu, J. Cryst. Growth **312**, 2999 (2010).

[28] B. R. Sahu and L. Kleinman, Phys. Rev. B **69**, 193101 (2004).

[29] M. Ceriotti, F. Pietrucci, and M. Bernasconi, Phys. Rev. B **73**, 104304 (2006).

[30] Yanlu Li, Weiliu Fan, Honggang Sun, Xiufeng Cheng, Pan Li, and Xian Zhao, J. Appl. Phys. **107**, 093506 (2010).

[31] Y. Ohmachi and N. Uchida, J. Appl. Phys. **41**, 2307 (1970).

[32]J. Robertson, Rep. Prog. Phys. **69**, 327 (2006).
[33]E. Hartmann and l. Kovács, Phys. Status Solidi A **74**, 59 (1982).
[34]A. Watterich, K. Raksányi, O. R. Gilliam, R. H. Bartram, L. A. Kappers, H. Söthe, and J.-M. Spaeth, J. Phys. Chem. Solids **53**, 189 (1992)
[35]G. J. Edwards, O. R. Gilliam, R. H. Bartram, A. Watterich, R. Voszka, J. R. Niklas, S. Greulich-Weber, and J.-M. Spaeth, J. Phys. Condens. Matter **7**, 3013 (1995).
[36]V. Corregidor, D. Martín y Marero, J. M. Gil, and E. Diéguez, Europhys. Lett. **67**, 247 (2004).
[37]R. C. Vilão, J. M. Gil, H. V. Alberto, J. Piroto Duarte, N. Ayres de Campos, A. Weidinger, M. V. Yakushev, and S. F. J. Cox, Physica B **326**, 181 (2003).
[38]A. I. Mansour, Z. Salman, K. H. Chow, I. Fan, P. J. C. King, B. Hitti, J. Jung, and S. P. Cottrell, Phys. Rev. Lett. **100**, 257602 (2008).
[39]P. A. Thomas, J. Phys. C **21**, 4611 (1988).
[40]P. E. Blöchl, Phys. Rev. B **50**, 17953 (1994).
[41]G. Kresse and J. Hafner, Phys. Rev. B **47**, 558 (1993).
[42]G. Kresse and J. Hafner, Phys. Rev. B **49**, 14251 (1994).
[43]G. Kresse and J. Furthmüller, Phys. Rev. B **54**, 11169 (1996).
[44]J. P. Perdew, K. Burke, and M. Ernzerhof, Phys. Rev. Lett. **77**, 3865 (1996).
[45]H. Monkhorst and J. Pack, Phys. Rev. B **13**, 5188 (1976).
[46]A. G. Marinopoulos, K. van Benthem, S. N. Rashkeev, S. J. Pennycook, and S. T. Pantelides, Phys. Rev. B **77**, 195317 (2008).
[47]H. Jónsson, G. Mills, and K. W. Jacobsen, in *Classical and Quantum Dynamics in Condensed Phase Simulations*, edited by B. J. Berne, G. Ciccotti, and D. F. Coker (World Scientific, Singapore, 1998), p. 385.
[48]K. H. Chow, B. Hitti, and R. F. Kiefl, in *Identification of Defects in Semiconductors*, edited by M. Stavola, Semiconductors and Semimetals, Vol. 51A (Academic Press, San Diego, 1998), pp. 137–207, treatise edited by R. K. Willardson and E. R. Weber.
[49]M. C. Lynch, S. P. Cottrell, P. J. C. King, and G. H. Eaton, Physica B **326**, 270 (2003).
[50]R. Abela, A. Amato, C. Baines, X. Donath, R. Erne, D. C. George, D. Herlach, G. Irminger, I. D. Reid, D. Renker, G. Solt, D. Suhi, M. Werner, and U. Zimmermann, Hyperfine Interact. **120/121**, 575 (1999).
[51]H. Jain and A. S. Nowick, Phys. Status Solidi A **67**, 701 (1981).
[52]J. S. Lord, Physica B **374**, 472 (2006).
[53]J. M. Gil, P. J. Mendes, L. P. Ferreira, H. V. Alberto, R. C. Vilão, N. Ayres de Campos, A. Weidinger, Y. Tomm, Ch. Niedermayer, M. V. Yakushev, R. D. Tomlinson, S. P. Cottrell, and S. F. J. Cox, Phys. Rev. B **59**, 1912 (1999).
[54]S. F. J. Cox, Rep. Prog. Phys. **72**, 116501 (2009).
[55]Hengshan Qiu, Bernd Meyer, Yuemin Wang, and Christof Wöll, Phys. Rev. Lett. **101**, 236401 (2008).
[56]R. C. Vilão, J. M. Gil, A. Weidinger, H. V. Alberto, J. Piroto Duarte, N. Ayres de Campos, R. L. Lichti, K. H. Chow, S. P. Cottrell, and S. F. J. Cox, Phys. Rev. B **77**, 235212 (2008).
[57]R. C. Vilão, J. M. Gil, A. Weidinger, H. V. Alberto, J. Piroto Duarte, B. F. O. Costa, N. Ayres de Campos, R. L. Lichti, K. H. Chow, S. P. Cottrell, and S. F. J. Cox, Physica B **404**, 888 (2009).
[58]R. L. Lichti, B. R. Carroll, J. E. Vernon, H. N. Bani-Salameh, K. H. Chow, I. Fan, M. Egilmez, R. C. Vilão, J. M. Gil, H. V. Alberto, J. Piroto Duarte, N. Ayres de Campos, S. P. Cottrell, and S. F. J. Cox, Physica B **404**, 827 (2009).
[59]J. B. Varley, A. Janotti, A. K. Singh, and C. G. Van de Walle, Phys. Rev. B **79**, 245206 (2009).